

Preparation of Bi₂O₃/ZnO/g-C₃N₄ and Its Photocatalytic Degradation for Rhodamine B and Methyl Orange Under Visible Light

Zahira Bano

School of Chemical Engineering, Nanjing University of Science & Technology, Nanjing 210094, PROC, China

Yousaf Saeed

Jiangsu University Zhenjiang, PROC, China

Mingzhu Xia

School of Chemical Engineering, Nanjing University of Science & Technology, Nanjing 210094, PROC, China

Wu Lei

School of Chemical Engineering, Nanjing University of Science & Technology, Nanjing 210094, PROC, China

Fengyun Wang*

School of Chemical Engineering, Nanjing University of Science & Technology, Nanjing 210094, PROC, China

Abstract

The ternary composite Bi₂O₃/ZnO/g-C₃N₄ was synthesized by simple co-precipitation method. Its potential application as a promising photocatalytic activity for rhodamine B (RhB) and methyl orange (MO) has been reported. The prepared samples were characterized by the various techniques such as X-ray diffraction, fourier transform infrared spectroscopy, x-ray photoelectron spectroscopy, UV-vis spectroscopy, transmission electron microscopy and scanning electron microscopy. These characterization and degradation results showed that the Bi₂O₃ and g-C₃N₄ have been distributed on the surface of ZnO nano-particles. Loading of the Bi₂O₃ and g-C₃N₄ nanosheets on n-ZnO surfaces resulted in an increased surface area and light absorption ability, which is due to the formation of the Bi₂O₃/ZnO/g-C₃N₄ heterojunctions between the semiconductors.

Keywords: Photocatalyst; Heterogeneous catalyst; Heterojunction; Photodegradation; Photostability; Semiconductor; Ternary composite; Photocatalysis.



CC BY: [Creative Commons Attribution License 4.0](https://creativecommons.org/licenses/by/4.0/)

1. Introduction

Today, solar energy, radiant light, and heat from the sun are the most abundant clean energy sources. Thus extensive research studies and development of materials that can utilize solar energy and use it for environment pollution management are essential. In this case, advanced oxidation processes (AOPs) play an important role via oxidation and reduction reactions. The photocatalysis phenomena created great interest in the scientific community, as it is the most suitable way to solve the wastewater-related issues. Especially, to get rid of the organic pollutants which are being produced by the textile, pharmaceutical and other related industries [1].

To date, TiO₂ and ZnO as semiconductor photocatalysts with a large band gap of 3.2eV have been tremendously investigated under the UV light illumination, which is only 3-5% of the solar light. Less cost and easy synthesis of n-ZnO as compared to the TiO₂ made it a potential photocatalyst for industries [2]. However, just because of the wide band gap and quick recombination of charge carriers, limits its universal use as a photocatalyst. It has attracted much attention in nano-scale based materials because of its unique chemical properties as compared to bulk ZnO [3]. The use of ZnO is also limited in the visible region because of its wide band gap energy, which causes fast recombination of electron-hole pairs, that results in low photocatalytic activity [4]. Therefore many efforts have been carried out in order to develop new techniques for the modification of ZnO photocatalysis. Such as doping with metals [5], transition metals [6], non-metals [7], controllable structure and morphology [1]. It is true that these metals are much expensive and not readily available. Therefore, it is necessary to find an inexpensive material that possess similar characteristics.

In the previous literature, Bismuth oxides were used as a promising photocatalytic semiconductors. Subramanian et al. reported the facile fabrication of Bi₂O₃-ZnO photocatalyst in UV light irradiation [8]. Nevertheless, Bi₂O₃ has some drawbacks due to the fast recombination of electron-hole pairs, low quantum yield and very poor adsorption properties, which badly effects its practical use.

Similarly, bulk g-C₃N₄ is n-type organic semiconductor with a band gap of ~2.7 eV, that was proven to be an effective photocatalyst for hydrogen and oxygen production through water splitting under visible light illumination [9]. Bulk g-C₃N₄ was reported as a layered semiconductor and can be transformed into thin nano-sheets. The g-C₃N₄ nano-sheets have large surface consists of very thin layers. Which gives excellent conductivity, with very less resistance between these layers. This characteristic makes g-C₃N₄ NS as a promising material for the construction of

*Corresponding Author: wangfy@njust.edu.cn

heterogeneous catalyst with other semiconductors [10]. Another way to control the recombination rate and to improve the photocatalysis in visible light is to build ternary heterojunctions between semiconductors with suitable band potentials. [11].

Herein, a novel ternary composite $\text{Bi}_2\text{O}_3/\text{ZnO}/\text{g-C}_3\text{N}_4$ was prepared by simple one step co-precipitation method. The morphology of the synthesized ternary composite was investigated by the scanning electron microscope and transmission electron microscope. Its photocatalytic activity was carried out on methyl orange and rhodamine B dye, which was drastically improved by the introduction of the ternary photocatalyst as compared to bare ZnO and Bi_2O_3 . Meanwhile, the effect of $\text{g-C}_3\text{N}_4$ concentrations and photo stability on the photocatalytic degradation was also investigated.

2. Experimental Section

2.1. Materials

Zinc acetate dihydrate ($\text{C}_4\text{H}_6\text{O}_4\text{Zn}\cdot 2\text{H}_2\text{O}$), oxalic acid dihydrate ($\text{C}_2\text{H}_2\text{O}_4\cdot 2\text{H}_2\text{O}$), bismuth (III) nitrate pentahydrate ($\text{Bi}(\text{NO}_3)_3\cdot 5\text{H}_2\text{O}$), polyvinylpyrrolidone (PVP), melamine ($\text{C}_3\text{H}_6\text{N}_6$), nitric acid (HNO_3), hydrochloric acid (HCL) were obtained commercially from Sigma Aldrich Chemical Cooperation. All the chemicals used in this experiment are reagent grade purity and used without any further process. Deionized water was used throughout the process.

2.2. Heat Treatment Preparation of Bi_2O_3

Modified Bi_2O_3 was prepared by the following procedure [12], a fixed amount of (1.94g) of $\text{Bi}(\text{NO}_3)_3\cdot 5\text{H}_2\text{O}$ poured into 10ml of HNO_3 (0.5M) nitric acid just to abdicate hydroxylation of Bi^{3+} ions. Respectively (0.2g) of polyvinylpyrrolidone PVP was then added in the above solution and stirred for 30 minutes. The role of PVP here is to control the morphology and size of the particles of Bi_2O_3 . (0.5M) NaOH solution was slowly added drop by drop into the above solution until its pH reaches 11. After that the mixture was stirred for 2 hours at room temperature, then heated for 3 hours at 90°C until its color changes to bright yellow and then followed by calcination process at 430°C for 2 hours. This yellow precipitate was filtered, washed with distilled water and alcohol several times and then dried at 70°C for 24 hours.

2.3. Preparation of $\text{g-C}_3\text{N}_4$ Nanosheets

Modified $\text{g-C}_3\text{N}_4$ was prepared according to literature [13]. Shortly (15g) of melamine was used as a source raw material and calcined at 530°C for 5 hours with a heating rate of $6^\circ\text{C}/\text{min}$. Then the received product was ground into powder and calcined again at 550°C for 4 hours with the same heating rate to derive nano-sheets (NS) of $\text{g-C}_3\text{N}_4$. The obtained NS were sonicated for 10 hours in isopropanol to get the single layered $\text{g-C}_3\text{N}_4$. The final product was filtered, washed with distilled water and ethanol several times. Then dried at 70°C for 12 hours.

2.4. Preparation of ZnO

The synthesis procedure of the n-ZnO micro-rods (n-ZnO MR) is the modified version of the previous report [14]. n-ZnO MR were constructed with ZnO nano-spheres via solvothermal assisted heat treatment method. Briefly, (27mmol) of Zinc acetate dihydrate ($\text{C}_4\text{H}_6\text{O}_4\text{Zn}\cdot 2\text{H}_2\text{O}$) and (27mmol) of oxalic acid dihydrate ($\text{C}_2\text{H}_2\text{O}_4\cdot 2\text{H}_2\text{O}$) were added into (70ml) of absolute ethanol under constant magnetic stirring until the following mixture forms a gel. Then this gel is transferred to the stainless steel autoclave (100ml). The sealed autoclave was then heated at 100°C for 5 hours. When the reaction was completed, the MR were collected, filtered and washed with double distilled water for five times. Finally dried at 70°C for 12 hours.

2.5. Preparation of $\text{Bi}_2\text{O}_3/\text{ZnO}/\text{g-C}_3\text{N}_4$ Ternary Composite

The $\text{Bi}_2\text{O}_3/\text{ZnO}/\text{g-C}_3\text{N}_4$ was electronically assembled by the following procedure. Briefly fixed amount of Bi_2O_3 and n-ZnO were separately dissolved into the 15ml Polyethylglycol (PEG-200) and distilled water. Bi_2O_3 solution was magnetically stirred for 1 hour at room temperature to give some time for solubility of the Bi_2O_3 in PEG and n-ZnO MR was dissolve in 20ml ethanol for half an hour. $\text{g-C}_3\text{N}_4$ was poured into 10ml of HCl to get the protonation of $\text{g-C}_3\text{N}_4$ and left for an hour. Afterwards these three solutions were mixed together and magnetically stirred for 3 hours at room temperature. Then the received product was filtered, washed and dried at 80°C for 24 Hours. Samples with percentage of 30%, 40% and 50% $\text{g-C}_3\text{N}_4$ were recorded by BZG1, BZG2 and BZG3 for further use.

3. Characterization

The powder X-ray diffraction(XRD) patterns of the samples were examined using the Bruker D8 X-ray diffractometer with $\text{Cu } \alpha$ radiation ($\lambda=0.1506$ nm, voltage= 40 kv, electrical current = 40 mA, $2\theta= 20-80^\circ$). The morphologies of the samples were investigated by the field emission electron microscope (FESEM-JEOL JSM-6380LV), and transmission electron microscope (TEM-JEM-2010). A UV-Vis Spectrometer (Thermo Fisher EV220, USA) was used to analyze the performance of the photocatalyst. Fourier transform infrared (FT-IR) analysis was recorded by FT-IR spectrometer (Thermo Fisher, NicoletisS10, FTIR spectrometer USA). X-ray photoelectron spectroscopy (XPS) analysis was measured using a PHI Quantra II Spectrometer, Al α (1486.6 eV) radiation.

3.1. Photocatalytic Activity

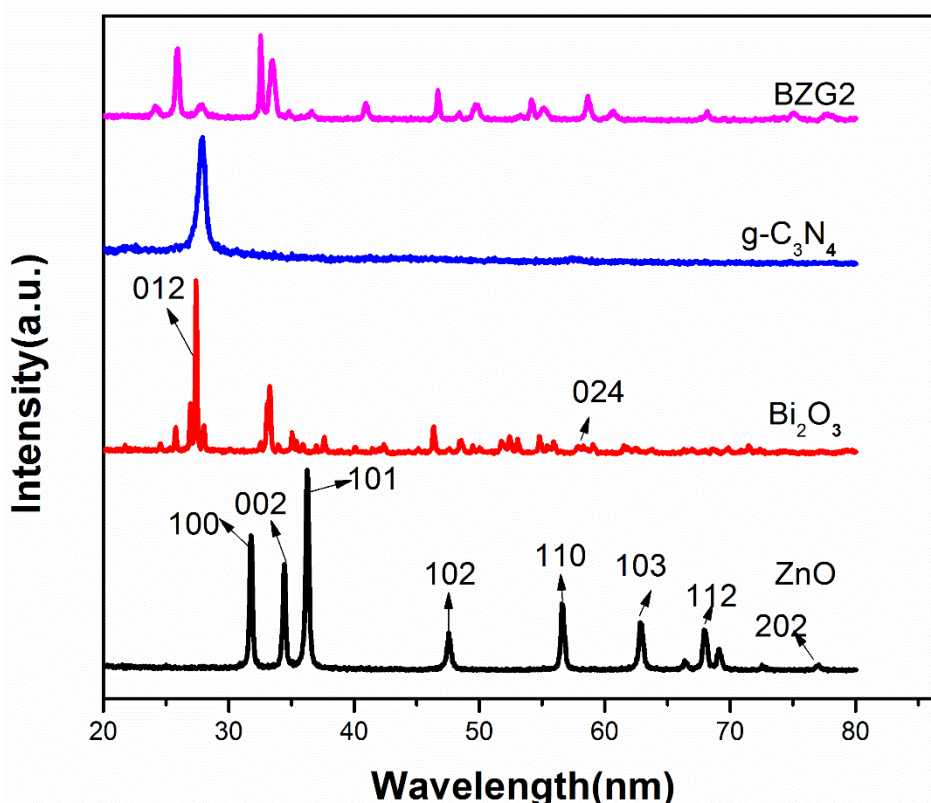
The photocatalytic measurements were performed in the visible region by using a BL-GHX-1D photochemical reactor (Shanghai Billion Instrument Co. Ltd). The photocatalytic runs were carried in cylindrical Pyrex glass tube that was put in the photochemical reactor. In each run, 10mg of the prepared catalyst was dispersed into the 80ml of RhB solution (15mg/l). The photocatalytic performance was then measured by irradiating the prepared solutions by a 500W xenon electric lamp with a cut off filter ($\lambda \geq 450\text{nm}$) to avoid the UV-part of light and a cooling water system to control the temperature at 10°C . Before the Light irradiation an adsorption-desorption reaction was carried out under stirring in the dark for 40 minutes to ensure the adsorption-desorption equilibrium. Then the Xenon 500W lamp was turned on and 5ml of suspension was taken out from solution after every 10 minutes' interval. The Suspension was then centrifuged at 11500 rpm for 15 minutes to collect the catalyst. The photocatalytic activity was analyzed at the maximum absorption wavelength of 664nm for (RhB) and 464nm for (MO) by the UV-vis spectrophotometer (Thermo fisher EV220 USA).

4. Results and Discussions

4.1. XRD

The XRD graphs of the bare ZnO, Bi_2O_3 , g- C_3N_4 and ternary composite BZG2 are represented in [figure.1](#). The diffraction peak at 2Theta with lattices parameter shown in [Figure.1](#) which is in agreement with the JCPDF code number (01-079-0206) of wurtzite structure of ZnO having hexagonal crystal geometry. In general, the diffraction peaks of Bi_2O_3 presented in [Figure.1](#) are monoclinic geometrical shape which agree with the JCPDF code number of monoclinic structure of Bi_2O_3 (01-081-0465). From the XRD of BZG2, peaks of hexagonal structure of ZnO appeared at 32.6° (100), 33.8° (002), 46.8° (101), 58.9° (110), 68.0° (112), 77.6° (202) and monoclinic peaks of Bi_2O_3 can be found at 27.8° (012) and 57.8° (024). The appearance of g- C_3N_4 peaks was not found in the ternary composite BZG2, mainly because of the very low quantity of the g- C_3N_4 . There was no other impurity found.

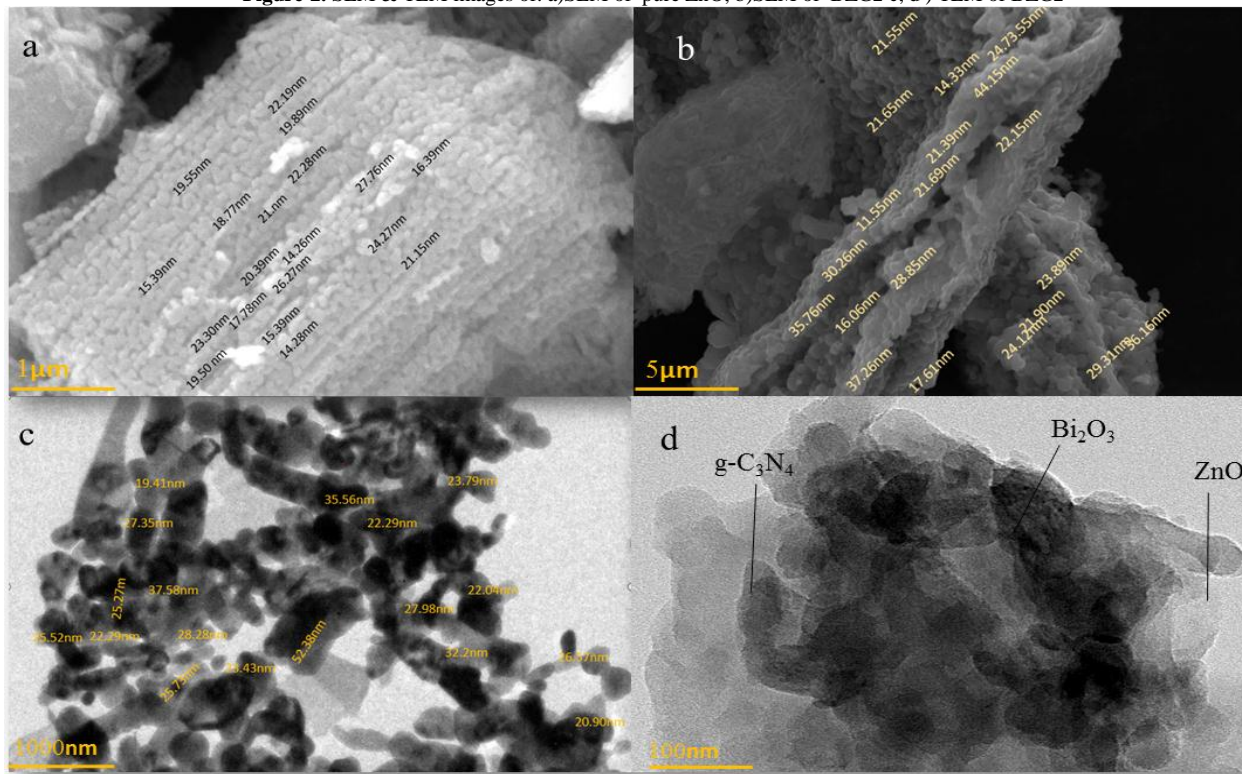
Figure-1. XRD graph of pure ZnO, pure Bi_2O_3 , g- C_3N_4 and BZG2



4.2. SEM & TEM

The morphology of the prepared samples was analyzed by the FESEM & TEM. From SEM images it can be seen that the structure of the bare zinc oxide is like micro-rods embedded by nano-spheres enclosed in a hexagonal structure presented in [Figure.2a](#). The size of the nano-spheres estimations are 14.26, 14.27, 15.39, 16.39, 17.7, 19.55, 21.15, 22.19, 27.76nm and so on ([Figure.2a](#)). The average mean particle size of the nano-spheres of ZnO was found to be 18.94nm from the SEM images by using statistical calculations. The results showed that the mean size obtained from the SEM and TEM images of the ternary composite is larger than the simple n-ZnO MR as shown in [Figure.2b&2c](#). The size of the nanoparticles of the ternary composite were 11.31, 36.29, 22.15, 14.33, 16.46, 24.73, 30.10, 21.90, 44.15, 20.77, 33.17, 36.16, 29.31nm and so on ([Figure.2b](#)). The average mean size of ternary composite BZG2 obtained was 25.79 nm. The increment in the particle size is due to the loading of the Bi_2O_3 and g- C_3N_4 NS on the surface of ZnO nano-spheres.

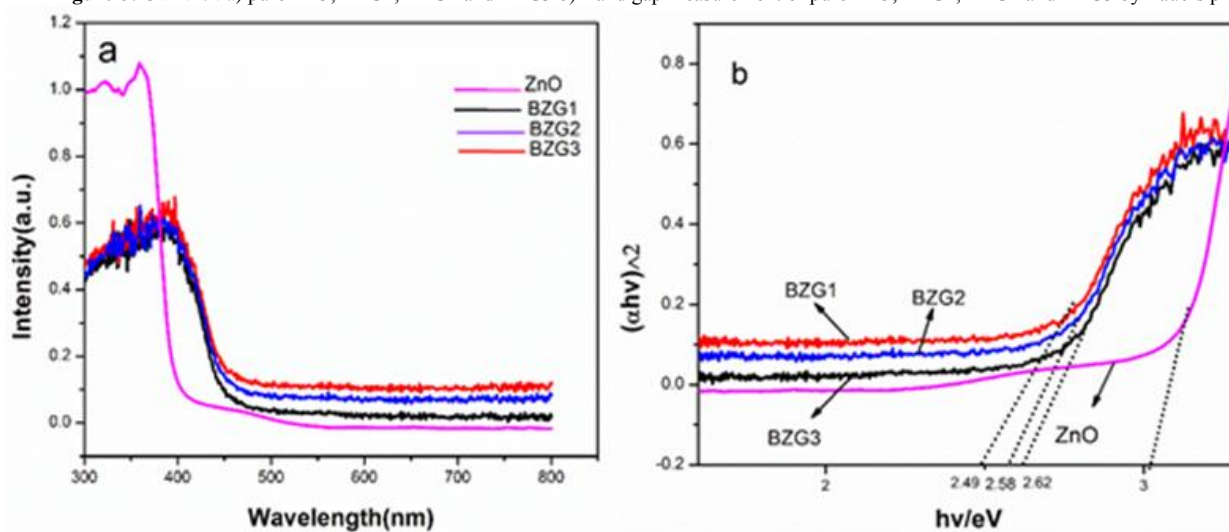
Figure-2. SEM & TEM images of: a) SEM of pure ZnO, b) SEM of BZG2 c, d) TEM of BZG2



4.3. Optical Studies

The UV-vis absorption spectra of the prepared samples were examined in order to determine their light absorption characteristics. Figure.3 shows the UV-vis absorption spectra of the pure ZnO, BZG1, BZG2 and BZG3 composites. Compared to the pure ZnO, BZG ternary composite has higher UV-vis light absorbance. Thus according to the Tauc's plot [15] obtained from the UV-vis absorption spectra source data, the band gaps of BZG composites are narrower than pure n- ZnO . That is due to the loading of Bi_2O_3 and $\text{g-C}_3\text{N}_4$ nanosheets on the surface of n-ZnO nano-spheres, which has a considerable impact on the electronic properties and improve the separation of photogenerated charge carriers. The band gap observed for the pure n-ZnO is 3eV.01, BZG1 is 2.62eV, BZG2 is 2.49eV and BZG3 2.58eV as shown in Figure.3b. The lowest band gap is observed when the concentration of $\text{g-C}_3\text{N}_4$ was 40% of pure ZnO. When the concentration of $\text{g-C}_3\text{N}_4$ was increased further the recombination of charge carriers increased, that is due to the large concentration of $\text{g-C}_3\text{N}_4$ nanosheets on n-ZnO surface, which limits the electron-hole pair separation. The UV-vis absorption spectra of liquid used samples are shown in figure-S3.

Figure-3. UV-Vis : a) pure ZnO, BZG1, BZG2 and BZG3 b) Band gap measurement of pure ZnO, BZG1, BZG2 and BZG3 by Tauc's plot

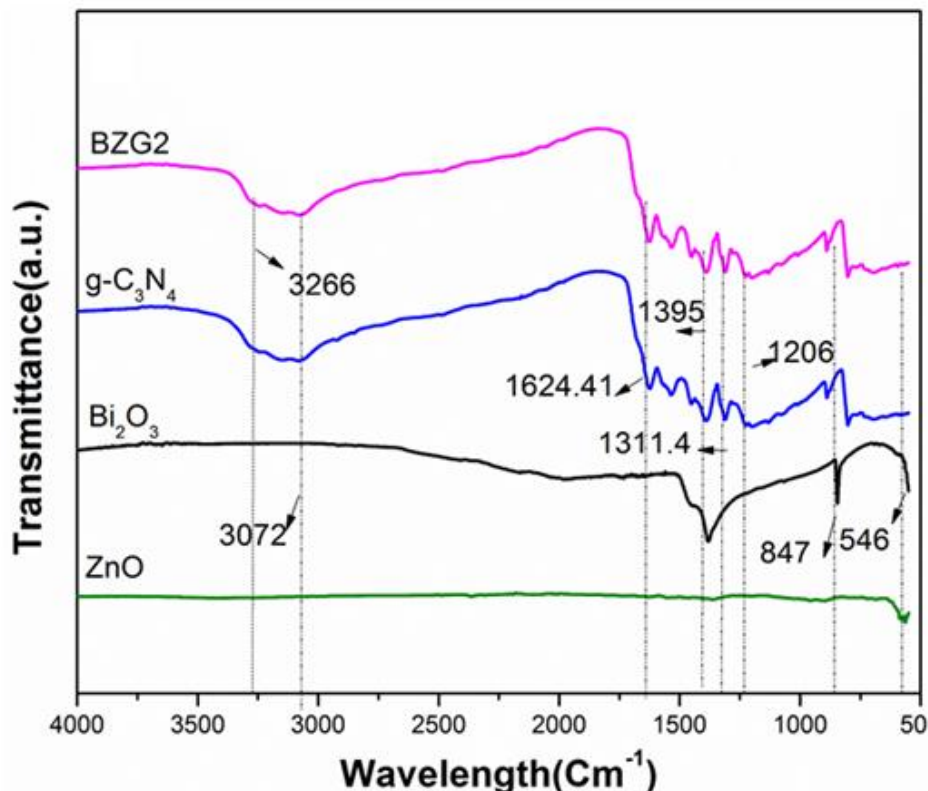


4.4. FTIR

It is further confirmed by the FT-IR analysis as it can be seen in Figure.4. In the spectrum of bare ZnO, the peaks appeared at 3414 cm^{-1} (Figure.S1) corresponds to the O-H bond and the peaks appeared around 525 cm^{-1} corresponds to the Zn-O bond respectively. The peaks found at $1600\text{-}1118\text{ cm}^{-1}$ (Figure.S1) are due to the presence of the C=O, C-O functional groups, which is the result of the oxidative decomposition of the organic dyes [16]. The peaks located at $847, 546\text{ cm}^{-1}$, seen at the spectrum of Bi_2O_3 corresponds to the stretching vibrations of Bi-O and Bi-

O-Bi [17-19] (Figure.4). In the spectrum of g-C₃N₄ NS (Figure.4) the peaks appeared at 1206, 1311.4, 1395, 3072, and 1624.41 cm⁻¹ shows the typical stretching modes of C-N heterocycles [20]. Thus all the peaks of ZnO and Bi₂O₃ and g-C₃N₄ can be clearly seen in the BZG2 ternary composite (Figure.4). Slight difference in the peaks may be due to the formation of the Ternary composite

Figure-4. FT-IR of pure ZnO, Bi₂O₃ and BZG2

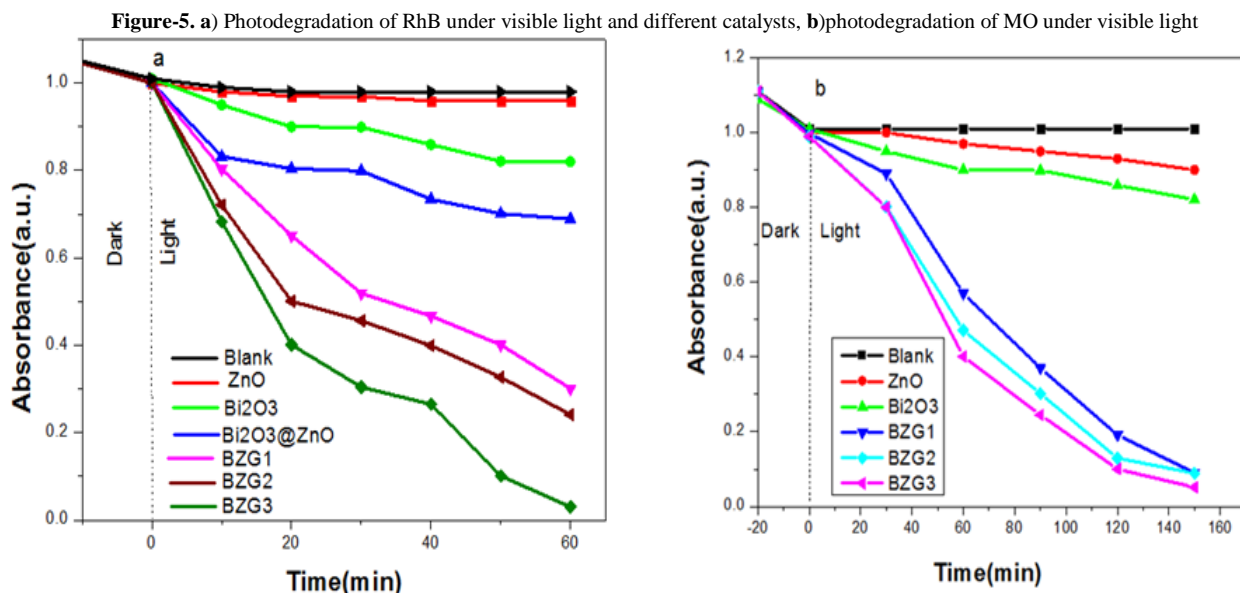


4.5. XPS

The chemical composition of Bi₂O₃/ZnO/g-C₃N₄ ternary composite and the chemical state of the elements were investigated by XPS analysis. XPS survey spectrum indicates the presence of zinc, oxygen, bismuth, carbon and nitrogen elements as shown in Figure.S2. Figure.S2. (a) shows the O1s spectrum of ZnO, Bi₂O₃ and BZG2. The peaks at 528.41eV, 528.61eV and 529.88eV (Figure.S2.a) attributed to the Bi-O, Zn-O and C-O bonds in Bi₂O₃, ZnO and BZG2 respectively [21-23]. Peaks located at 530.24eV and 531.24eV are assigned to the adsorbed H₂O on the surface. 531.24eV is associated with oxygen(O₂⁻) ions in the oxygen deficient regions or Zn-OH groups. Zn2p_{3/2} and Zn2p_{1/2} signals from the XPS Zn2P spectrum were noticed at characteristics binding energies of about 1019.74eV and 1042.93eV (Figure.S2.b). The small difference may be because of the Zn defects in BZG2 [24]; [21]. Hence the peaks found at 157.02eV and 162.32 eV resembles to the Bi4f (Figure.S2c) of Bi₂O₃ [12]. Three peaks at 284.13eV, 283.73eV and 287.06eV are attributed to C1s (Figure.S2.e) of g-C₃N₄ NS. The constituent peaks at 397.59 eV, 399.40 eV and 403.01 eV are assigned to the N1s (Figure.S2.d) of g-C₃N₄.

4.6. Photocatalytic Degradation

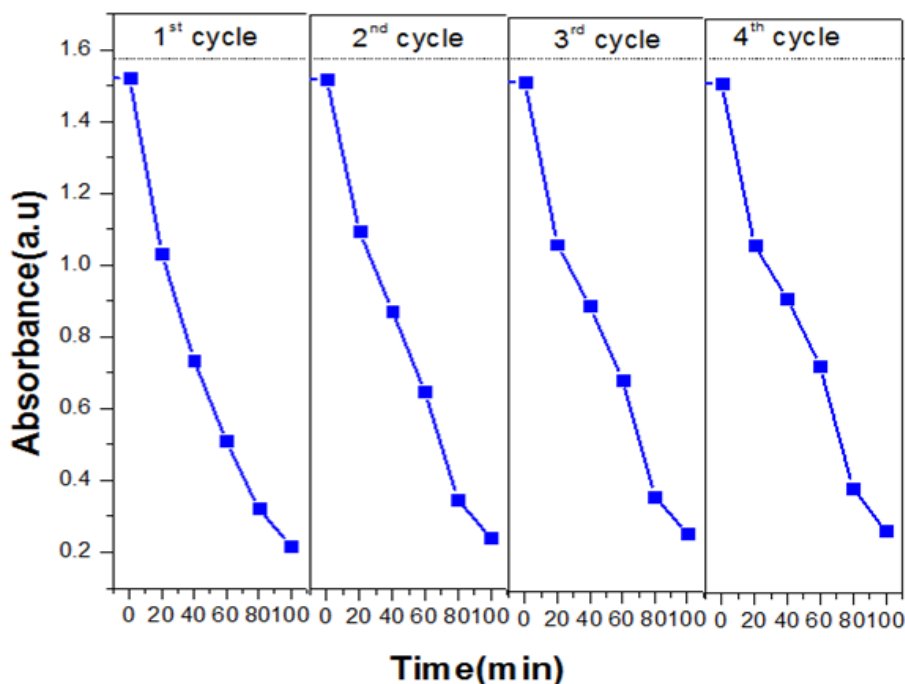
The photocatalytic degradation of RhB and MO under visible light irradiation is shown in Figure-5. Dye is resistant to the self-photocatalysis and a small decrease in dye concentration was observed when it was kept for stirring in dark after the addition of the catalyst, which is due to the adsorption of the dye on the catalyst surface. Rhodamine B undergoes 95% degradation in the presence of visible light lamp (Figure.5a). But pure ZnO, Bi₂O₃, and Bi₂O₃-ZnO undergoes only 10, 20 and 30 percent degradation under visible light irradiation within 60 minutes. Whereas, the degradation rates of BZG1, BZG2 and BZG3 are 70.1, 95.1 and 75.6 percent. So based on these results it can be concluded that the enhanced photocatalytic activity is because of the presence of Bi₂O₃ and C₃N₄ in the BZG ternary composite. To determine the efficiency of the catalyst, degradation of methyl orange was also carried out under the same conditions as RhB. The degradation time for each dye was different. The photocatalytic degradation of MO was investigated at 10mg/l of dye solution by ZnO, BZG1, BZG2, and BZG3 as shown in (Figure.5b). The MO dye was degraded 95% in 150 minutes. The best result was observed by BZG2 sample.



4.6.1. Photostability

To find out the photostability of the ternary composite under visible light irradiation, BZG2 was used to perform the photocatalytic activity for the RhB dye. After each cycle, the photocatalyst was washed with acetone and used again. In Figure.6, it is shown that the photocatalytic performance of the BZG2 shows an effective stability towards the RhB dye under visible light irradiation. The catalyst was recycled four times. It was observed that after continuous recycles, the catalyst still shows good photocatalytic activity. The XRD graphs of the recycled samples are shown in Figure.S4.

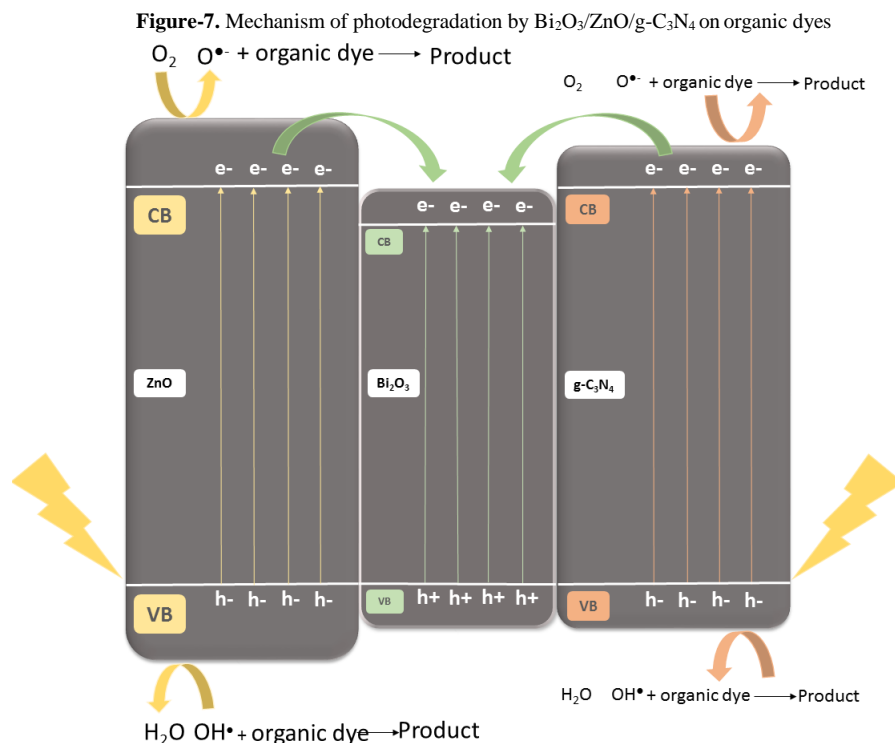
Figure-6. recycled photocatalytic activity of BZG2 on RhB dye.



4.6.2. Mechanism

On the basis of above-mentioned information, a proposed mechanism of $\text{Bi}_2\text{O}_3/\text{ZnO}/\text{g-C}_3\text{N}_4$ ternary composite is presented in Figure.7. Two main reasons are highlighted in order to explain the enhanced behavior of $\text{Bi}_2\text{O}_3/\text{ZnO}/\text{g-C}_3\text{N}_4$. i) UV-vis light absorbance is increased by the presence of the Bi_2O_3 , which itself is a good visible light photocatalyst. When it was loaded with n-ZnO, it created a bridge for the electron transportation from n-ZnO to Bi_2O_3 , which in turn facilitate the better separation of charge carriers. II) The photogenerated electrons from the CB of $\text{g-C}_3\text{N}_4$ migrates to the CB of Bi_2O_3 due to the lower CB potential of Bi_2O_3 . The holes from VB of Bi_2O_3 moves to the VB of $\text{g-C}_3\text{N}_4$ that is because of the lower VB potential of $\text{g-C}_3\text{N}_4$. Due to the presence of $\text{g-C}_3\text{N}_4$, the separation efficiency is further improved [25]. This charge separation is also investigated by the UV-vis diffuse absorbance spectra. The efficient separation of electron-hole pairs results in improved photocatalytic performance. The Hydroxyl radical ($\bullet\text{OH}$) acts as a main reactive component which is responsible for the photocatalytic degradation of organic dyes [8]. The photo-induced electrons react with the O_2 molecules that were adsorbed on the surface of the $\text{Bi}_2\text{O}_3/\text{ZnO}/\text{g-C}_3\text{N}_4$ composite to yield the $\text{O}_2^{\bullet-}$. The photo-induced holes then react with H_2O to produce ($\bullet\text{OH}$)

radicals. These photogenerated ions of $O_2^{\bullet-}$ and $(\bullet OH)$ are responsible for the degradation of organic dye adsorbed on the surface of $Bi_2O_3/ZnO/g-C_3N_4$. Therefore, the prepared composite of $Bi_2O_3/ZnO/g-C_3N_4$ presents enhanced photocatalytic activity as compared to bare ZnO and Bi_2O_3-ZnO .



5. Conclusion

In this study a ternary composite $Bi_2O_3/ZnO/g-C_3N_4$ was successfully synthesized by loading varying amount of $g-C_3N_4$ nanosheets on the ZnO surface and Bi_2O_3 with simple co-precipitation method. In comparison to the bare n-ZnO, Bi_2O_3 and Bi_2O_3-ZnO , ternary composite $Bi_2O_3/ZnO/g-C_3N_4$ shows high photocatalytic performance towards the rhodamine B and methyl orange under the visible light lamp. The presence of Bi_2O_3 would be favorable for the enhancement of photocatalytic activity, because it can absorb the visible light to produce active species. It can capture photo-induced electrons and holes to promote charge carrier separation. The introduction of $g-C_3N_4$ (NS) acts as a charge transfer center. The synergistic effect could be concluded as the formation of a heterojunction between p-type semiconductor and n-type semiconductors. Which hence improves the charge separation due to the formation of n-p-n junction chemistry among the three semiconductors. The present work may provide a route to prepare novel and highly promising ternary semiconductor composites for the remediation of organic pollutants present in water.

Acknowledgement

This work was supported by the National Natural Science Foundation of P. R. China (51242001, 51572127 and 5122351).

References

- [1] Lan, S., Liu, L., Li, R., Leng, Z., and Gan, S., 2014. "Hierarchical Hollow Structure ZnO: Synthesis, Characterization, and Highly Efficient Adsorption/Photocatalysis toward Congo Red." *Industrial & Engineering Chemistry Research*, vol. 53, pp. 3131-3139. 2014/02/26. Available: <http://dx.doi.org/10.1021/ie404053m>
- [2] Daneshvar, N., Salari, D., and Khataee, A. R., 2004. "Photocatalytic degradation of azo dye acid red 14 in water on ZnO as an alternative catalyst to TiO₂." *Journal of Photochemistry and Photobiology A: Chemistry*, vol. 162, pp. 317-322. 2004/03/15/. Available: <http://www.sciencedirect.com/science/article/pii/S1010603003003782>
- [3] Lu, W., Gao, S., and Wang, J., 2008. "One-Pot Synthesis of Ag/ZnO Self-Assembled 3D Hollow Microspheres with Enhanced Photocatalytic Performance." *The Journal of Physical Chemistry C*, vol. 112, pp. 16792-16800. 2008/10/30. Available: <http://dx.doi.org/10.1021/jp803654k>
- [4] Gomez-Solis, C., Ballesteros, J. C., Torres-Martínez, L. M., Juárez-Ramírez, I., Díaz Torres, L. A., Elvira Zarazua-Morin, M., and Lee, S. W., 2015. "Rapid synthesis of ZnO nano-corncoobs from Nital solution and its application in the photodegradation of methyl orange." *Journal of Photochemistry and Photobiology A: Chemistry*, vol. 298, pp. 49-54. 2015/02/01/. Available: <http://www.sciencedirect.com/science/article/pii/S1010603014004316>

- [5] Xu, L., Xiao, S., Zhang, C., Zheng, G., Su, J., Zhao, L., and Wang, J., 2014. "Optical and structural properties of Sr-doped ZnO thin films." *Materials Chemistry and Physics*, vol. 148, pp. 720-726. 2014/12/15/. Available: <http://www.sciencedirect.com/science/article/pii/S0254058414005392>
- [6] Zhang, Z., Yi, J. B., Ding, J., Wong, L. M., Seng, H. L., Wang, S. J., Tao, J. G., Li, G. P., Xing, G. Z., *et al.*, 2008. "Cu-Doped ZnO Nanoneedles and Nanonails: Morphological Evolution and Physical Properties." *The Journal of Physical Chemistry C*, vol. 112, pp. 9579-9585. 2008/07/01. Available: <http://dx.doi.org/10.1021/jp710837h>
- [7] Zong, X., Sun, C., Yu, H., Chen, Z. G., Xing, Z., Ye, D., Lu, G. Q., Li, X., and Wang, L., 2013. "Activation of Photocatalytic Water Oxidation on N-Doped ZnO Bundle-like Nanoparticles under Visible Light." *The Journal of Physical Chemistry C*, vol. 117, pp. 4937-4942. 2013/03/14. Available: <http://dx.doi.org/10.1021/jp311729b>
- [8] Balachandran, S. and Swaminathan, M., 2012. "Facile Fabrication of Heterostructured Bi₂O₃-ZnO Photocatalyst and Its Enhanced Photocatalytic Activity." *The Journal of Physical Chemistry C*, vol. 116, pp. 26306-26312. 2012/12/20. Available: <http://dx.doi.org/10.1021/jp306874z>
- [9] Wang, X., Maeda, K., Thomas, A., Takanabe, K., Xin, G., Carlsson, J. M., Domen, K., and Antonietti, M., 2008. "A metal-free polymeric photocatalyst for hydrogen production from water under visible light." *Nature Materials*, vol. 8, p. 76. 11/09/online. Available: <http://dx.doi.org/10.1038/nmat2317>
- [10] Xu, J., Zhang, L., Shi, R., and Zhu, Y., 2013. "Chemical exfoliation of graphitic carbon nitride for efficient heterogeneous photocatalysis." *Journal of Materials Chemistry A*, vol. 1, pp. 14766-14772. Available: <http://dx.doi.org/10.1039/C3TA13188B>
- [11] Ren, P., Fan, H., and Wang, X., 2013. "Solid-state synthesis of Bi₂O₃/BaTiO₃ heterostructure: preparation and photocatalytic degradation of methyl orange." *Applied Physics A*, vol. 111, pp. 1139-1145. June 01. Available: <https://doi.org/10.1007/s00339-012-7331-6>
- [12] Anandan, S., Lee, G.-J., Chen, P.-K., Fan, C., and Wu, J. J., 2010. "Removal of Orange II Dye in Water by Visible Light Assisted Photocatalytic Ozonation Using Bi₂O₃ and Au/Bi₂O₃ Nanorods." *Industrial & Engineering Chemistry Research*, vol. 49, pp. 9729-9737. 2010/10/20. Available: <http://dx.doi.org/10.1021/ie101361c>
- [13] Liao, G., Chen, S., Quan, X., Yu, H., and Zhao, H., 2012. "Graphene oxide modified g-C₃N₄ hybrid with enhanced photocatalytic capability under visible light irradiation." *Journal of Materials Chemistry*, vol. 22, pp. 2721-2726. Available: <http://dx.doi.org/10.1039/C1JM13490F>
- [14] Deng, Q., Duan, X., Ng, D. H. L., Tang, H., Yang, Y., Kong, M., Wu, Z., Cai, W., and Wang, G., 2012. "Ag Nanoparticle Decorated Nanoporous ZnO Microrods and Their Enhanced Photocatalytic Activities." *ACS Applied Materials & Interfaces*, vol. 4, pp. 6030-6037. 2012/11/28. Available: <http://dx.doi.org/10.1021/am301682g>
- [15] Radecka, M., Rekas, M., Trenczek-Zajac, A., and Zakrzewska, K., 2008. "Importance of the band gap energy and flat band potential for application of modified TiO₂ photoanodes in water photolysis." *Journal of power sources*, vol. 181, pp. 46-55.
- [16] Finocchio, E., Cristiani, C., Dotelli, G., Stampino, P. G., and Zampori, L., 2014. "Thermal evolution of PEG-based and BRIJ-based hybrid organo-inorganic materials. FT-IR studies." *Vibrational Spectroscopy*, vol. 71, pp. 47-56.
- [17] Yan, Y., Zhou, Z., Cheng, Y., Qiu, L., Gao, C., and Zhou, J., 2014. *Template-free fabrication of ??- And ??-Bi₂O₃ hollow spheres and their visible light photocatalytic activity for water purification* vol. 605, pp. 102-108.
- [18] Jiang, H.-Y., Liu, J., Cheng, K., Sun, W., and Lin, J., 2013. "Enhanced Visible Light Photocatalysis of Bi₂O₃ upon Fluorination." *The Journal of Physical Chemistry C*, vol. 117, pp. 20029-20036. 2013/10/03. Available: <http://dx.doi.org/10.1021/jp406834d>
- [19] Zhang, L., Wang, W., Yang, J., Chen, Z., Zhang, W., Zhou, L., and Liu, S., 2006. "Sonochemical synthesis of nanocrystallite Bi₂O₃ as a visible-light-driven photocatalyst." *Applied Catalysis A: General*, vol. 308, pp. 105-110. 2006/07/10/. Available: <http://www.sciencedirect.com/science/article/pii/S0926860X06002973>
- [20] Xiang, Q., Yu, J., and Jaroniec, M., 2011. "Preparation and Enhanced Visible-Light Photocatalytic H₂-Production Activity of Graphene/C₃N₄ Composites." *The Journal of Physical Chemistry C*, vol. 115, pp. 7355-7363. 2011/04/21. Available: <http://dx.doi.org/10.1021/jp200953k>
- [21] Motaung, D. E., Mhlongo, G. H., Nkosi, S. S., Malgas, G. F., Mwakikunga, B. W., Coetsee, E., Swart, H. C., Abdallah, H. M. I., Moyo, T., *et al.*, 2014. "Shape-Selective Dependence of Room Temperature Ferromagnetism Induced by Hierarchical ZnO Nanostructures." *ACS Applied Materials & Interfaces*, vol. 6, pp. 8981-8995. 2014/06/25. Available: <http://dx.doi.org/10.1021/am501911y>
- [22] Parmigiani, F., Shen, Z. X., Mitzi, D. B., Lindau, I., Spicer, W. E., and Kapitulnik, A., 1991. "O 1s core levels in $\text{Bi}_{1-x}\text{Sr}_x\text{CaCu}_2\text{O}_{8+\delta}$ single crystals." *Physical Review B*, vol. 43, pp. 3085-3090. 02/01/. Available: <https://link.aps.org/doi/10.1103/PhysRevB.43.3085>
- [23] Liu, H., Cao, W., Su, Y., Wang, Y., and Wang, X., 2012. "Synthesis, characterization and photocatalytic performance of novel visible-light-induced Ag/BiOI." *Applied Catalysis B: Environmental*, vol. 111-112, pp. 271-279. 2012/01/12/. Available: <http://www.sciencedirect.com/science/article/pii/S0926337311004784>

- [24] Xu, C., Xu, G., Liu, Y., and Wang, G., 2002. "A simple and novel route for the preparation of ZnO nanorods." *Solid State Communications*, vol. 122, pp. 175-179. 2002/04/01/. Available: <http://www.sciencedirect.com/science/article/pii/S003810980200114X>
- [25] Dang, X., Zhang, X., Chen, Y., Dong, X., Wang, G., Ma, C., Zhang, X., Ma, H., and Xue, M., 2015. "Preparation of β -Bi₂O₃/g-C₃N₄ nanosheet p-n junction for enhanced photocatalytic ability under visible light illumination." *Journal of Nanoparticle Research*, vol. 17, p. 93. 2015/02/13. Available: <https://doi.org/10.1007/s11051-014-2808-1>

Appendix

Figure-S1. Zoomed FTIR of pure ZnO and Bi₂O₃-ZnO

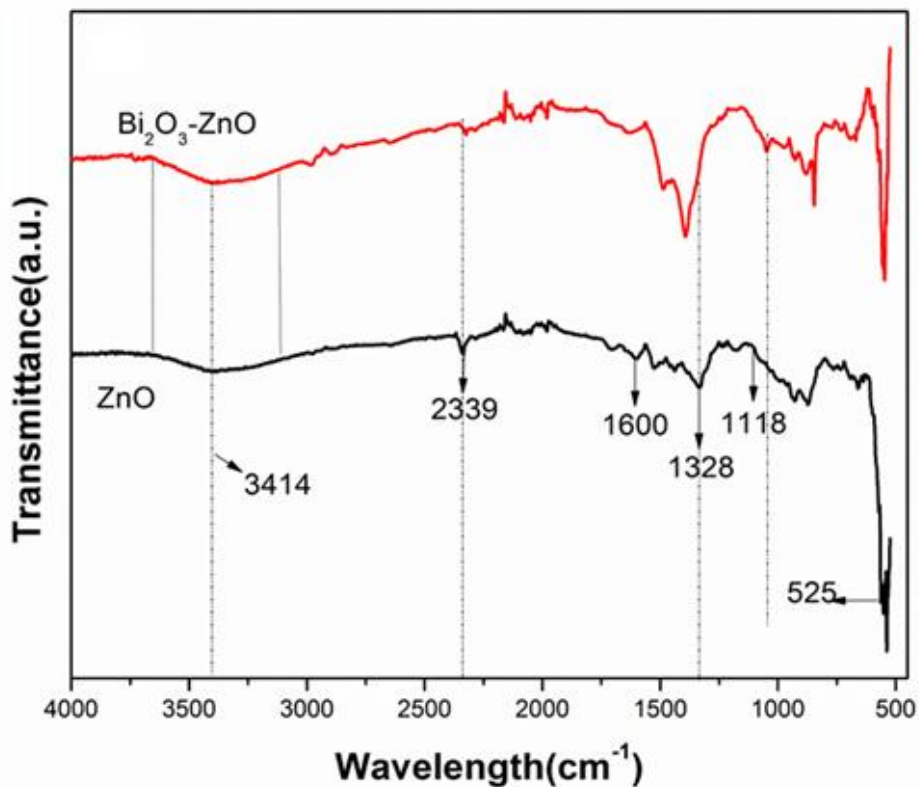


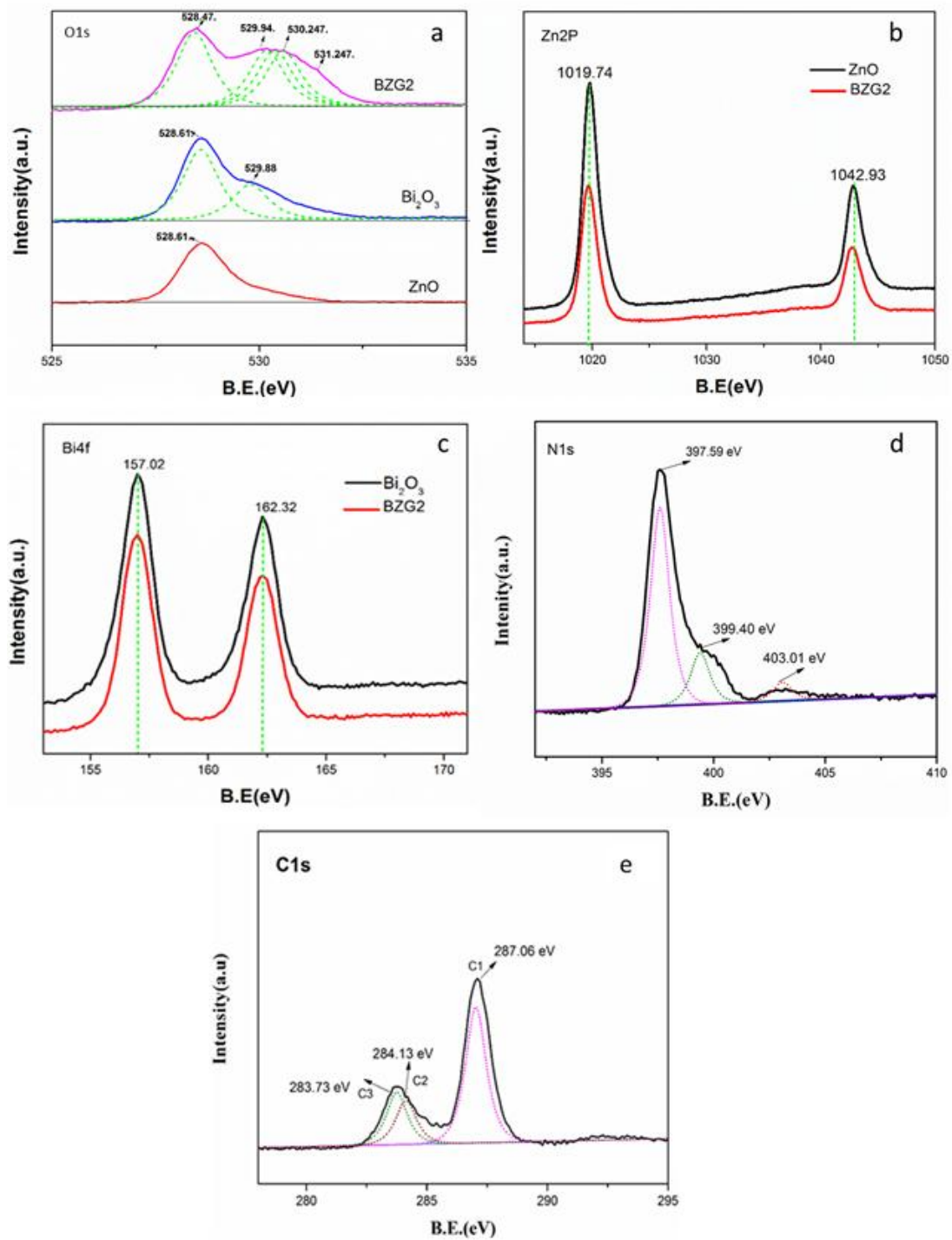
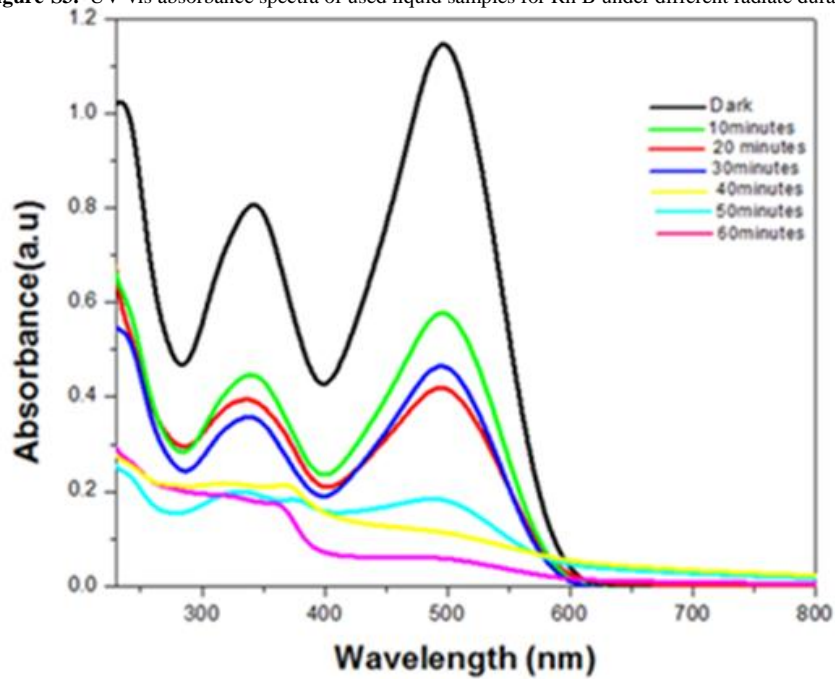
Figure-S2. a) XPS of pure ZnO, Bi₂O₃ and BZG2 a) O1s, b) Zn2p c) Bi 4f d) N1s e) C1s

Figure-S3. UV-vis absorbance spectra of used liquid samples for Rh B under different radiate duration**Figure-S4.** XRD of Recycled samples